



Direct photon production in Au+Au collisions at $\sqrt{s_{NN}} = 200$ GeV at STAR

Chi Yang (for the STAR Collaboration)¹

Department of Modern Physics, University of Science and Technology of China, Hefei, Anhui 230026, China

Brookhaven National Laboratory, Upton, NY 11973, USA

Abstract

We present the direct photon production for $1 < p_T < 10$ GeV/c derived from continuum in the dielectron invariant mass region $0.1 < M_{ee} < 0.3$ GeV/c² from one billion $\sqrt{s_{NN}} = 200$ GeV Au+Au events taken in year 2010 and 2011. A clear excess in the invariant yield compared to the number of binary collision scaled $p + p$ reference is observed in the p_T range 1-4 GeV/c. Model calculations with contributions from thermal radiation and initial hard parton scattering are consistent within uncertainties with the direct photon invariant yield.

Keywords: dielectron, direct photon, thermal radiation, Quark-Gluon Plasma (QGP)

1. Introduction

Direct photons and dileptons are clean probes to study the fundamental properties of a hot and dense medium created in ultra-relativistic heavy-ion collisions. Due to minimal interactions with the strongly interacting medium, they can bring the information of the whole time evolution and dynamics of the medium. The PHENIX direct-photon measurements in Au+Au, d+Au and $p + p$ collisions at $\sqrt{s_{NN}} = 200$ GeV showed that for $p_T < 4$ GeV/c an enhanced yield above the number of binary collision (N_{coll}) scaled $p + p$ production is observed in Au+Au while there is no similar enhancement in d+Au collisions. In the high p_T range, the invariant yield in Au+Au collisions is consistent with N_{coll} scaled $p + p$ production and the NLO pQCD predictions [1, 2]. The results from ALICE in Pb+Pb and $p + p$ collisions at $\sqrt{s_{NN}} = 2.76$ TeV showed an excess in Pb+Pb over the scaled $p + p$ for $p_T < 4$ GeV/c [3] while the yield measured by CMS collaboration in Pb+Pb collisions follows the scaled $p + p$ results and NLO pQCD predictions in the photon transverse energy (E_T) range 20-80 GeV [4]. These measurements indicate that in the low p_T range, there are contributions from other sources rather than initial hard parton scattering. The study on direct photons opens two kinematic windows. One is the low p_T range for the in-medium effect study. The other one is the high p_T range for the hard process research. With the comparison to model prediction, some key parameters of the QGP matter such as initial temperature can be obtained [5].

There are two methods for direct photon measurement. One is the real photon method in which one measures all inclusive photons and then subtracts the hadron decayed photons from them. The other one is the virtual photon method in which one measures the virtual photon by their associate dielectron pairs and then deduces the direct photon from the relationship between virtual photon and direct photon. The latter is used in this article. The dielectron

¹A list of members of the STAR Collaboration and acknowledgements can be found at the end of this issue.

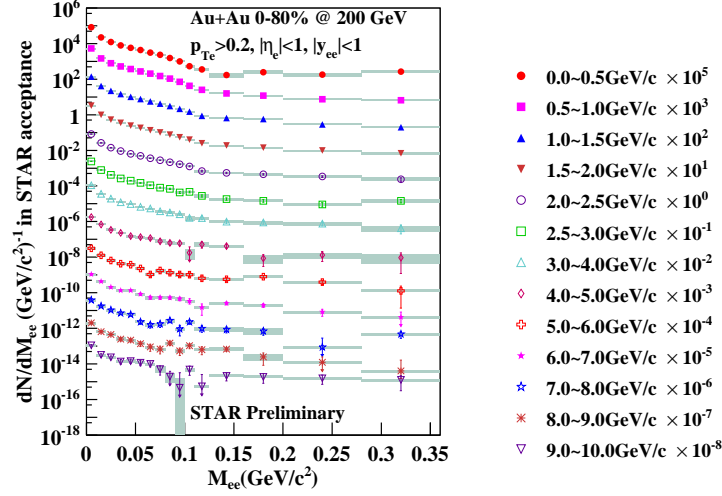


Figure 1. Dielectron invariant mass spectra in the low mass range for different p_T slices. The spectra in different p_T slices are scaled by different factors for clarification. The error bars and the shaded bands represent the statistical and systematic uncertainties, respectively.

measurement in Au+Au collisions at 200 GeV at STAR from year 2010 data has been published recently [6]. The preliminary results on dielectron production in $p + p$ collisions at 200 GeV from year 2012 can be found in [7]. In this article, we focus on the measurement of direct photon in Au+Au collisions at 200 GeV.

2. Analysis

The data used in this analysis are from Au+Au collisions at $\sqrt{s_{NN}} = 200$ GeV collected in year 2010 (Run10) and 2011 (Run11). There are 258 million and 488 million minimum bias (0-80%) events from Run10 and Run11, respectively, passing bad run rejections and vertex selections. The main subsystems used for electron identification are the Time Projection Chamber (TPC) [8] and the Time-of-Flight detector (TOF) [9] for the minimum-bias events. With the requirements on the particle energy loss (dE/dx) measured by TPC close to electron expected dE/dx and time-of-flight measured by TOF close to the speed of light, electron samples can be selected with high purity. The electron purity is about 95% in Au+Au minimum bias collisions. The dielectron invariant mass spectra are obtained separately with Run10 and Run11 datasets. The final results are then combined point-to-point according to their relative statistical uncertainties. To improve the statistics at high p_T , we use the Barrel Electro-Magnetic Calorimeter (BEMC) [10] triggered events taken in Run11. The 39 million BEMC triggered events used in this analysis are equivalent to 5389 million minimum bias triggered events. The BEMC trigger significantly enhances the capability of STAR for high p_T dielectron measurement. For BEMC triggered electrons, additional requirements on the ratio of momentum measured by the TPC to the energy deposited in the BEMC are utilized. The electron purity can reach about 80% for BEMC triggered electron sample. The dielectron invariant mass spectrum in this paper are within STAR acceptance ($p_T^e > 0.2$ GeV/c, $|\eta^e| < 1$, $|y^{ee}| < 1$) and corrected for efficiency, in which p_T^e is the electron p_T , η^e is the electron pseudo-rapidity, and y^{ee} is the rapidity of electron-positron pairs. The dielectron invariant mass spectra in different p_T ranges are shown in Fig. 1. The results for $p_T < 5$ GeV/c are the combined results from Run10 and Run11 minimum bias data. The results for $p_T > 5$ GeV/c are from the BEMC triggered data. More dielectron analysis details and results can be found in [6, 11].

A contribution from internal conversion of direct photons is expected. The relation between real photon and the associated e^+e^- pair production can be described as Eq. 1 [12, 13].

$$\frac{dN_{ee}}{dM} = \frac{2\alpha}{3\pi} \sqrt{1 - \frac{4m_e^2}{M^2}} \left(1 + \frac{2m_e^2}{M^2}\right) \frac{S(M)}{M} dN_\gamma \quad (1)$$

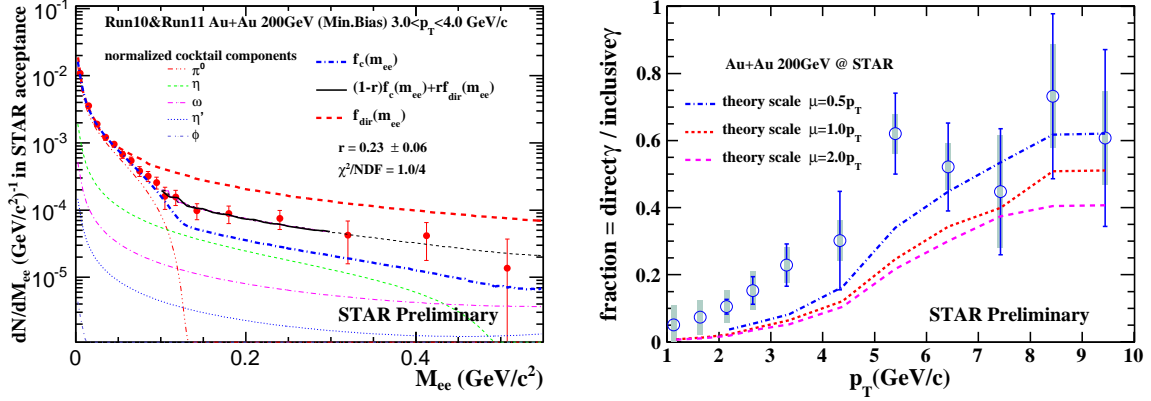


Figure 2. Left panel shows the two-component function fit on Au+Au dielectron spectra for $0.1 < M_{ee} < 0.3 \text{ GeV}/c^2$ at $3 < p_T < 4 \text{ GeV}/c$. Red dashed line is f_{dir} while blue dashed-dot line is $f_{cocktail}$. The black solid line is the fit to the data for $0.1 < M_{ee} < 0.3 \text{ GeV}/c^2$. The black dashed line is the extrapolation of the fit function outside the fit range. Right panel shows the ratio of direct photon to the inclusive photon compared with the NLO pQCD prediction (see text). The error bars and the shaded bands represent the statistical and systematic uncertainties, respectively.

In Eq. 1, M is the mass of the virtual photon or the e^+e^- pair, α is the fine structure constant, and $S(M)$ describes the difference between real photon process and virtual photon process. In this analysis, this factor $S(M)$ is assumed to be 1 in the range $M_{ee} < 0.3 \text{ GeV}/c^2$, $p_T > 1 \text{ GeV}/c$. Based on Eq. 1, the measurement of dielectron spectrum in the low mass region will deduce the production of direct photons [14].

The direct photon yields are extracted by fitting the dielectron invariant mass spectra in the low mass region with two components. One component is the contribution from hadron cocktail and the other one comes from direct photon internal conversion. In the fit function $(1-r)f_{cocktail} + rf_{dir}$, r is the ratio of direct photon to inclusive photon. The $f_{cocktail}$ is the normalized cocktail while the f_{dir} is the normalized internal conversion from direct photon passing STAR acceptance in different p_T ranges. The left panel of Fig. 2 shows an example of the two-component fit. The uncertainties shown in the figure are the quadrature sum of statistical and systematic uncertainties. The blue dashed-dot line and red-dashed lines represent the normalized cocktail and internal conversion from direct photon, respectively. The black solid line is the fit to the data at $0.1 < M_{ee} < 0.3 \text{ GeV}/c^2$. The black dashed line is the extrapolation of the fit function outside the fit range. Right panel of Fig. 2 shows the ratio of direct photon to inclusive photon compared with the NLO pQCD prediction. The curves represent $T_{AA}d\sigma_{\gamma}^{NLO}(p_T)/N_{\gamma}^{inclusive}(p_T)$, showing the scale dependence of the theory [15], in which T_{AA} is the nuclear overlapping factor. The $d\sigma_{\gamma}^{NLO}(p_T)$ is the p_T -differential invariant cross section of direct photon obtained from [16]. The $N_{\gamma}^{inclusive}(p_T)$ is the STAR measurement which is in form of $F/(\frac{2\alpha}{3\pi})/(2\pi p_T dp_T dy)$, in which F is the normalization factor of f_{dir} . The data show consistency with NLO pQCD calculation within uncertainties at $p_T > 4 \text{ GeV}/c$. A clear enhancement in data compared to the calculation for $1 < p_T < 4 \text{ GeV}/c$ is observed.

Figure 3 shows the invariant yield of the direct photons in Au+Au collisions at 200 GeV. In the left panel, the open circles are the direct photon invariant yields measured from STAR 200 GeV 0-80% Au+Au collisions. The uncertainty is dominated by systematic uncertainty in the cocktail. The large systematic uncertainties in 1-2 GeV/c are due to the lack of η measurement in the corresponding p_T range. The η dN/dy and p_T input for cocktail simulation in this range are based on the extrapolation of the TBW model [17], while at $p_T > 2 \text{ GeV}/c$, it is constrained by the measurements. The triangles are the invariant cross sections in $p+p$ collisions at 200 GeV measured by PHENIX collaboration. They are parameterized by a power-law function, as shown in dotted line. The parameterized distribution is then scaled by the nuclear overlapping factor $T_{AA} = N_{bin}/42\text{mb} = 6.95\text{mb}^{-1}$ as shown in dashed line, and compared to the Au+Au results. For $1 < p_T < 4 \text{ GeV}/c$, the Au+Au results are clearly higher than the T_{AA} scaled $p+p$ results, while at high p_T the Au+Au yield is consistent with the scaled $p+p$ expectation. The right panel shows a comparison between STAR Au+Au data and model calculations done by Ralf Rapp et al. [5, 18]. The curves ‘‘QGP’’ stands for the contribution from QGP thermal radiation. The ‘‘ ρ ’’ and ‘‘hadron gas’’ represent contributions from in-medium ρ and

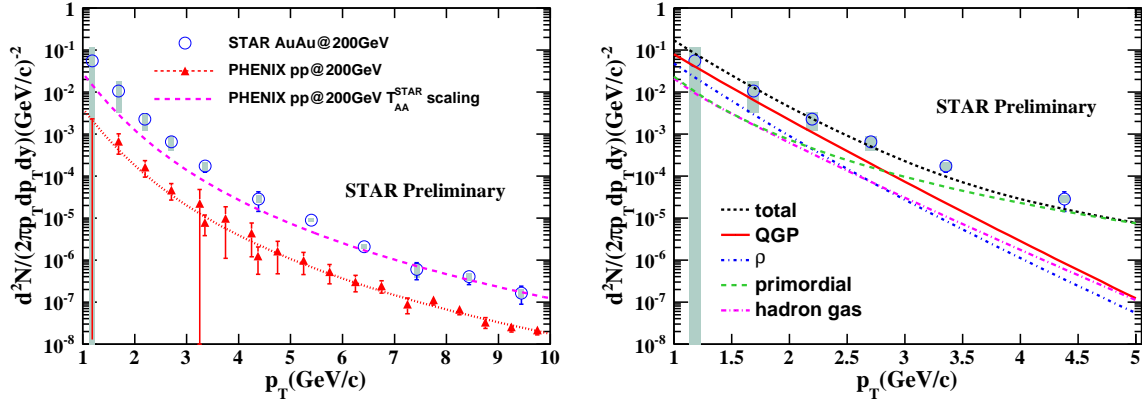


Figure 3. Left panel shows the direct photon invariant yield. The pink dashed curve represents a power-law fit to PHENIX 200 GeV $p + p$ cross section [14, 16], scaled by T_{AA} . Right panel shows the direct photon invariant yield compared to model predictions including the contributions from different sources [5, 18]. The statistical and systematic uncertainties are shown by the bars and bands, respectively.

other mesonic interactions in the hadronic gas, respectively. The “primordial” line depicts the contribution from the initial hard parton scattering. The comparison shows consistency between the model calculation and the measurement within uncertainties. In the low p_T range 1-4 GeV/c, the dominant sources are from thermal radiation while as the p_T increases to 4-5 GeV/c the initial hard parton scattering becomes the dominant source.

3. Conclusions

We measured direct photon production in Au+Au collisions at STAR at $\sqrt{s_{NN}} = 200$ GeV. The direct photon measurement based on virtual photon method is firstly extended to high p_T of 10 GeV/c. In the low p_T range 1-4 GeV/c, the production of direct photon can access the thermal radiation from QGP and hadron gas. The direct photon invariant yield in this range shows a clear excess in Au+Au over the number of binary collision scaled $p + p$ results. In the p_T range above 4 GeV/c, there is no clear enhancement observed. A model prediction which includes the contributions from thermal radiation and initial hard process is consistent with our direct photon yield within uncertainties.

References

- [1] A. Adare et al., Phys.Rev.C 87, 054907, 2013.
- [2] A. Adare et al., Phys.Rev.Lett. 104, 132301, 2010.
- [3] M. Wilde, Nucl.Phys.A 904-905, 573c-576c, 2013.
- [4] S. Chatrchyan et al., Phys.Lett.B 710, 256-277, 2012.
- [5] H. van Hees et al., Phys.Rev.C 84, 054906.
- [6] L. Adamczyk et al., Phys.Rev.Lett. 113, 022301, 2014.
- [7] Y. Guo for the STAR collaboration, WWND 2014 proceedings, arXiv:1407.6788.
- [8] M. Anderson et al., Nucl.Instrum.Meth.A 499, 659-678, 2003.
- [9] J. Adams et al., Phys.Rev.Lett. 94, 062301, 2005; J. Adams et al., Phys.Lett.B 616, 8, 2005.
- [10] M. Beddo et al., Nucl.Instrum.Meth.A 499, 725-739, 2003.
- [11] L. Adamczyk et al., Phys.Rev.C 86, 024906, 2012.
- [12] P. Lichard, Phys.Rev.D 51, 6017-6035, 1995.
- [13] L. G. Landsberg, Phys.Rept. 128, 301-376, 1985.
- [14] A. Adare et al., Phys.Rev.C 81, 034911, 2010.
- [15] L.E. Gordon and W. Vogelsang, Phys.Rev.D 48, 3136-3159, 1993.
- [16] S.S. Adler et al., Phys.Rev.Lett. 98, 012002, 2007.
- [17] Z. Tang et al., Phys.Rev.C 79, 051901, 2009.
- [18] R. Rapp, private communications.